IDETC2017-67550

TOWARDS OPTIMIZING DC LOADS FOR POWER GENERATION FROM ARBITRARILY EXCITED NONLINEAR VIBRATION ENERGY HARVESTERS

Quanqi Dai and Ryan L. Harne*

Department of Mechanical and Aerospace Engineering
The Ohio State University
Columbus, OH 43210, USA

*Corresponding Author, Email: harne.3@osu.edu

ABSTRACT

In order to effectively take advantage of stiffness nonlinearities in vibration energy harvesters, the harvesters must be appropriately designed to ensure optimum direct current (DC) power generation. Yet, such optimization has only previously been investigated for alternating current (AC) power generation although most electronics demand DC power for their functioning. Moreover, real world excitations contain stochastic contributions combined with periodic components that challenges conventional approaches of investigation that only give attention to the harmonic excitation parts. To fill in the knowledge gap, this research undertakes comprehensive simulations to begin formulating conclusive understanding on the relationships between rectified power generation and nonlinear energy harvester system characteristics when the platforms are subjected to realistic combinations of harmonic and stochastic excitations. According to the simulation results, the rectified power demonstrates clear dependence on the load resistance in the unique limiting cases of complete or no stochastic excitation. When the excitation vibrations include both harmonic and stochastic components, the optimal resistance to maximize DC power exhibits a smoothly correlated but nonlinear change between the limiting case values of the resistance. The results of this investigation provide direct evidence of the intricate relationships among peak DC power. optimal resistive loads, and the nonlinear energy harvester design, and encourage continued study for direct analytical expressions that define such relationships.

1 INTRODUCTION

The need for effective, on-site electrical energy resources to sustain the operation of sensors in industrial and automotive applications [1] [2] has motivated numerous studies of vibration energy harvesting. The vibration energy harvesters convert kinetic energy into useful electrical energy. As a result, the

harvesters must be appropriately designed to ensure optimum power generation under real world excitations that exhibit random and nonstationary characteristics [3] [4]. The idea of taking advantage of stiffness nonlinearities in vibration energy harvesters for large power generation cross broad frequency band has been investigated by numerous researchers and has been found to be a promising approach for harvesting ambient energy [5] [6] [7] [8] [9]. Smooth nonlinearities, and particularly bistable device configurations have revealed exceptional ability to harvest ambient input vibrations for power generation due to the large amplitude snap-through responses that oscillate between the two stable equilibria [10] [11] [12] [13].

Piezoelectric elements are one of the most common types of transducers to be utilized in vibration energy harvesters that are employed to harvest small scale ambient vibrations [14] [15], namely because of the relatively large power density achieved [15] than counterpart electromagnetic and electrostatic transducers [16] [17]. Erturk and Inman [18] has shown that the alternating current (AC) power output from linear energy harvesters exhibits clear dependence on the resistor values under harmonic excitations. Similarly, Stanton et al. [19] and Panyam and Daqaq [20] have shown that optimal electrical impedances exist to maximize AC power output from nonlinear piezoelectric energy harvester driven by harmonic inputs. The performance of piezoelectric nonlinear energy harvesters has also been evaluated considering random excitations [21] [22] [23], although optimization criteria were not then determined.

Yet, sensor nodes require direct current (DC) power [14], so that an AC-DC rectifier circuit is needed to interface between the piezoelectric elements and the (mostly resistive) loads of the sensors [24]. To meet this need, researchers have shown that the standard diode bridge rectifier, the synchronized switch harvesting on inductor, and the synchronized electric charge extraction circuits are all promising platforms [25] [26] [27] [28] [29]. Compared to the other two circuits, the standard diode

bridge rectifier does not require active control and can rectify the current to DC flow without significant power loss, which encourages the diode bridge consideration for developing optimized vibration energy harvester and circuit systems. Indeed, Shu and Lien [30] optimized the diode bridge circuit with the harmonically excited linear piezoelectric energy harvester revealing that the system can be enhanced by careful study.

Based on the results of the past research, the influences of resistive loads on the electrical performance of piezoelectric energy harvesters are crucial towards the energy conversion. Yet, the previous investigations have given attention to the roles of resistive loads on either AC power generation from linear energy harvesters or on DC power generation from nonlinear energy harvesters, where either harvester platform is subjected to harmonic excitations. Yet, DC power is required to sustain sensor functions [31] or charge a battery usable by an electronic device [32]. In addition, ambient vibrations, for example from human motion or vehicle operation [33], contain periodic characteristics with considerable noise which is more closely approximated by a combined harmonic and stochastic excitation. Under such conditions, the relationship between DC power output from nonlinear vibration energy harvesters and resistive loads has not yet been uncovered.

To fill in the knowledge gap, this research undertakes a first look at the influences of resistive load on governing the DC power generation from nonlinear piezoelectric energy harvester that are subjected to combined harmonic and stochastic excitations. Because bistable nonlinearities may lead to responses that is particularly favorable for large power generation, this research focuses on the electromechanical responses of bistable energy harvesters and the resulting DC power generation. The following sections first introduce the nonlinear energy harvester and corresponding governing equation model considered in this work. Then, results from numerical simulations are presented to explore the roles of the electrical load in tailoring the DC power generation from the nonlinear harvester when driven by combined harmonic and stochastic excitations. The final section consolidates the key observations of this study that motivate further analysis.

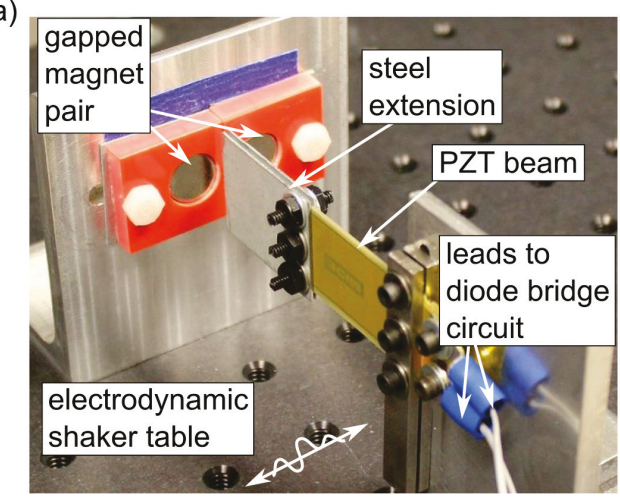
2 NONLINEAR ENERGY HARVESTER PLATFORM AND MODEL

2.1 Nonlinear energy harvester platform construction

A common method to introduce nonlinearity in the study of dynamical systems is through magnetoelastic structures [34] [35]. By the combination of magnets and elastic components, a full range of nonlinear characteristics exhibited by many nonlinear oscillators is enabled, while the adjustment of magnet positioning tunes the smooth nonlinear characteristics [36] [37]. Here, as shown in Fig. 1, the nonlinear energy harvester considered in this work is constructed by a piezoelectric cantilever (Midé Technology, PPA-2014) clamped in an aluminum mount, while a pair of steel extensions is connected to the free end of beam. The steel extensions are acted upon by a magnet pair that apply attractive forces opposing the direction of

linear elastic forces induced in the beam by displacement of the beam tip [34]. By tuning the position of magnets, namely the space between magnet pair Δ , and the distance from the cantilever free tip to magnets pair δ , the force acting on the beam can be changed so as to modify the nonlinearities of the system. For this research, the investigations give attention to the bistable nonlinearity due to the observations in the literature of beneficial performance of bistable structures for vibration energy harvesting purposes [10] [7] [13]. As shown in Fig. 1(b), a standard diode bridge rectifier is constructed by four 1N4148 diodes and is connected to the outputs of the piezoelectric beam to rectify the AC voltage \underline{v}_p into DC voltage \underline{v}_r across the

resistive load $\,R\,$ and smoothing capacitor $\,C_{r}\,.$



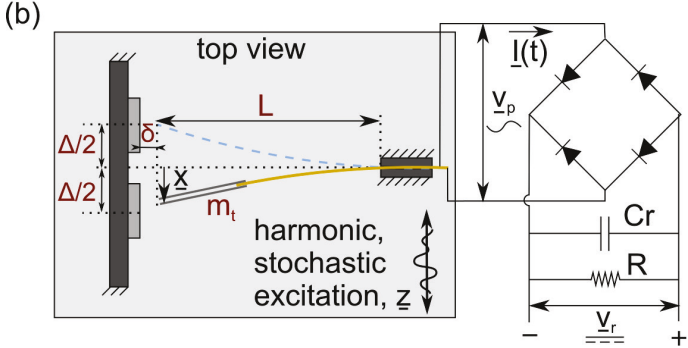


Figure 2. (a) Photograph and (b) schematic of the nonlinear energy harvester with diode bridge rectifier.

2.2Governing equations for the nonlinear energy harvester

Considering the development of a nonlinear energy harvesting for effectiveness in application, the responses of the structure are assumed to be dominated by the fundamental mode while higher order harmonics are sufficiently represented by a low-order Taylor series approximation of the nonlinear magnetic restoring forces. Therefore, the governing equations for the system are [12] [34] [38]

$$m\underline{\ddot{x}} + c\underline{\dot{x}} + k_1(1-p)\underline{x} + k_3\underline{x}^3 + \alpha\underline{v}_p = -m\underline{\ddot{z}}$$
 (1a)

$$C_{p}\dot{\underline{v}}_{p} + \underline{I} = \alpha \dot{\underline{x}} \tag{1b}$$

In Eq. (1), \underline{x} denotes the cantilever free tip relative displacement with respect to the motion of base \underline{z} to which the clamped end of the harvester and magnet pair are attached; m and c are the equivalent mass and viscous damping of the cantilever; k_1 is the linear stiffness, and k_3 is the nonlinear cubic stiffness; the influence of the magnetic forces upon the linear stiffness is quantified by parameter p. The value of the load parameter indicates the class of nonlinearity: p < 1 indicates that the harvester is monostable, while p > 1 indicates that the harvester is bistable [11] [34] [39]. The parameter α represents the electromechanical coupling; \underline{v}_p is the voltage across the piezoelectric element electrodes; C_p denotes the internal capacitance of the piezoelectric element; and the overdot operator represents differentiation with respect to time t.

The diode bridge rectifier incorporated in the harvester is constructed by four diodes, as shown in Fig. 1, which are assumed to be perfect, thus without forward voltage drop. The alternating current from the piezoelectric elements is denoted by $\underline{I}(t)$. The current is related to the rectified voltage \underline{v}_r through [30]

$$\underline{I}(t) = \begin{cases}
C_r \underline{\dot{v}}_r + \frac{\underline{v}_r}{R}; & \text{if } \underline{v}_p = \underline{v}_r \\
-C_r \underline{\dot{v}}_r - \frac{\underline{v}_r}{R}; & \text{if } \underline{v}_p = -\underline{v}_r \\
0; & \text{if } |\underline{v}_p| < \underline{v}_r
\end{cases} \tag{2}$$

For reducing the number of free parameters, the governing equations are nondimensionalized to:

$$x'' + \eta x' + (1 - p)x + \beta x^{3} + \kappa v_{p} = -z''$$
 (3a)

$$v_p' + I = \theta x' \tag{3b}$$

$$I(\tau) = \begin{cases} \gamma v_r' + \rho v_r; & \text{if } v_p = v_r \\ -\gamma v_r' - \rho v_r; & \text{if } v_p = -v_r \end{cases}$$

$$0; & \text{if } |v_p| < v_r$$
(3c)

The characteristic length and voltage are respectively defined as x_0 and V_0 , such that $x=\underline{x}\,/\,x_0$, $z=\underline{z}\,/\,x_0$, $v_p=\underline{v}_p\,/\,V_0$, $v_r=\underline{v}_r\,/\,V_0$. The time t is nondimensionalized by the system linear natural frequency $\omega_0=\sqrt{k_1\,/\,m}$, such that $\tau=\omega_0 t$. Other non-dimensional parameters are defined as follows: $\beta=k_3x_0^2\,/\,k_1$; $\eta=c\,/\,m\omega_0$; $\kappa=\alpha V_0\,/\,k_1x_0$; $\gamma=C_r\,/\,C_p$; $\rho=1\,/\,C_pR\omega_0$; $\theta=\alpha x_0\,/\,C_pV_0$

Here, ()' indicates differentiation with respect to non-dimensional time τ .

The base acceleration excitation includes harmonic and stochastic components

$$-z'' = a\cos\omega\tau + \sigma w(\tau) \tag{4}$$

such that $w(\tau)$ is a Gaussian white noise process with

$$\langle w(\tau) \rangle = 0$$
 and $\langle w(\tau)w(\tau + \tau_0) \rangle = \delta(\tau_0)$ (5)

and where σ is the normalized standard deviation of the noise [40]. Considering the harmonic excitation component, a is the normalized base excitation magnitude and ω is the angular frequency of excitation $\underline{\omega}_0$ normalized with respect to ω_0 . Thus, the absolute base excitation magnitude and standard deviation are $\underline{a} = ax_0k_1/m$ and $\underline{\sigma} = \sigma x_0k_1/m$, respectively.

3 RESULTS AND DISCUSSIONS

To evaluate the opportunity for optimizing the nonlinear energy harvester for DC power generation when the system is subjected to combined harmonic and stochastic excitations, a comprehensive set of simulations of the governing equations (3) is undertaken here. The fourth-order Runge Kutta algorithm is used to numerically integrate the equations via the MATLAB software. All simulations are conducted using parameters that pertain to the experimental nonlinear energy harvesting platform shown in Fig. 1. The corresponding parameter values for simulation are presented in Table.1.

Table 1. System parameters used in the simulations

m [g]	b	k_1	p [dim]	x_0
	[N.s/m]	[N/m]		[mm]
9.45	0.125	160	1.75	1
k_3	C_p [nF]	$C_r[\mu F]$	α [mN/V]	V_0 [V]
$[MN/m^3]$			[mN/V]	
33	96	10	1.4	1

3.1 Rectified power generation under pure harmonic excitation

The first assessment is the limiting case when the nonlinear energy harvester is subjected to pure harmonic excitation with amplitude \underline{a} =7.5 m/s². The normalized harmonic excitation frequencies are around the linear natural frequency, 0.2< $\underline{\omega}_0$ / ω_0 <2

Under such a harmonic excitation, Fig. 2(a) shows the mechanical responses of the harvester cantilever tip displacement amplitude, while the corresponding rectified power across resistor R are given in Fig. 2(b). According to the results, under this harmonic excitation scenario the displacement amplitude and DC power generation are small at low and high harmonic excitation frequencies. This is because the nonlinear

harvester undergoes intrawell responses associated with small amplitude motions around one of the two stable equilibria, which are not conducive for power generation. Fig. 2(a) also indicates that in the harmonic frequency range $0.5 < \underline{\omega}_0 / \omega_0 < 1$ snapthrough responses may be triggered, which leads to relatively large cantilever displacement amplitude and rectified power output. Three different resistor values are considered towards generating the results of Fig. 2, $R = [10^1, 5 \times 10^2, 10^4] \text{ k}\Omega$. As the resistor changes in value from $R = 10^1$ k Ω to $R = 5 \times 10^2$ $k\Omega$, Fig. 2(a) shows that the displacement amplitude is not significantly affected except for a slightly reduced frequency bandwidth for the snap-through responses. On the other hand, the rectified power generation corresponding to snap-through responses has appreciable improvements due to such increase of resistor value as shown in Fig. 2(b): the maximum DC power increases from 1.98 mW to 3.6 mW. However, further increase of the load resistor from $R = 5 \times 10^2$ k Ω to $R = 10^4$ k Ω reduced DC power to 0.24 mW, as shown in Fig. 2(b). Such variation of the rectified power that is associated with the snapthrough responses demonstrates the large sensitivity of the nonlinear energy harvester effectiveness according to the resistive load across which the direct current flows.

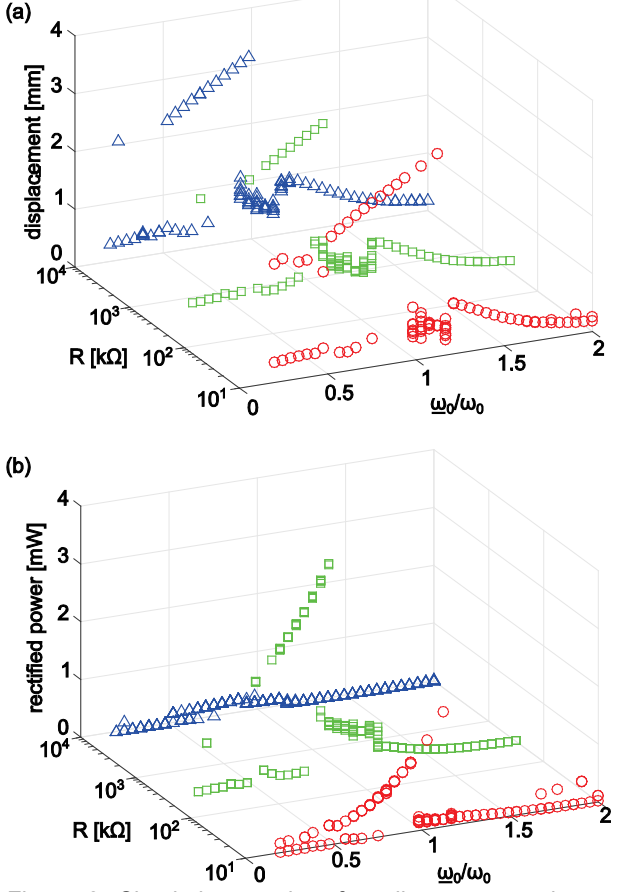


Figure 2. Simulation results of nonlinear energy harvester (a) cantilever tip harmonic displacement magnitude at the harmonic excitation frequency for three different resistor values and (b)

corresponding rectified power across each resistive load R , under pure harmonic excitation with amplitude \underline{a} =7.5 m/s².

According to the results presented in Fig. 2, intrawell and snap-through responses may coexist during the harmonic frequency range $0.5 < \underline{\omega}_0 / \omega_0 < 0.9$, so that it is important to characterize the DC power realized for different load resistances. To study the influence of the load resistance in greater detail, simulations are then conducted for specific harmonic excitation frequencies in the range of $0.5 \le \underline{\omega}_0 / \omega_0 \le 0.9$ while the resistance value is changed in small steps from $R = 10^1$ k Ω to $R = 10^4$ $k\Omega$. Comparatively, the simulation results in Fig. 3 reveal that the rectified power generation from snap-through responses is dramatically greater that the power provided from the intrawell dynamic response, in fact about one order of magnitude greater. The rectified power output due to snap-through responses demonstrates clear dependence on resistor values as shown in Fig. 3. The rectified power exhibits a maximum value when resistor values are from about $R = 10^2$ k Ω to $R = 5 \times 10^2$ $k\Omega$. In addition, it is observed from the set of results in Fig. 3 that the optimum resistor values decrease as the harmonic excitation frequency increases. In fact, this trend is similar to the trends of AC power generation using nonlinear bistable energy harvesters subjected to pure harmonic excitation [20]. This indicates that in the limiting case of pure harmonic excitation, maximal device mechanical response and power generation are strongly correlated, regardless of the electrical circuit composition.

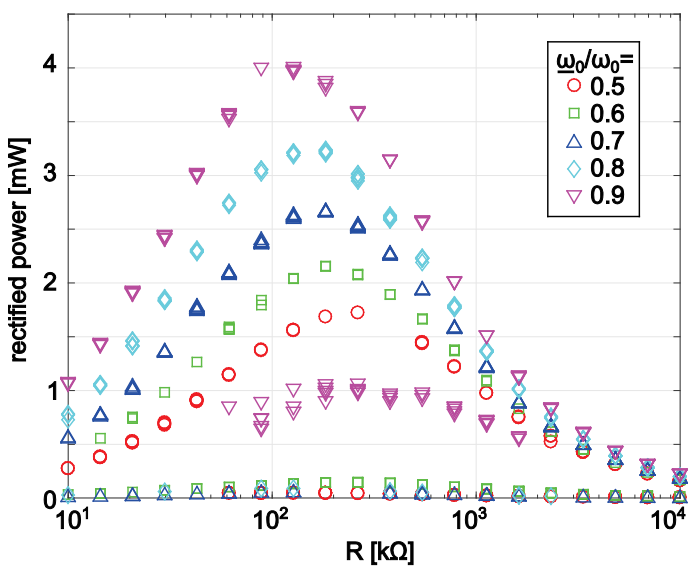


Figure 3. Simulation results for rectified power generation from the nonlinear energy harvester under harmonic excitation with amplitude \underline{a} =7.5 m/s² when harmonic frequency is at $\underline{\omega}_0$ / ω_0 =[0.5, 0.6, 0.7, 0.8, 0.9], as functions of load resistor R.

3.2 Rectified power generation under stochastic excitations

Having evaluated the limiting case of DC generation from pure harmonic excitation, simulations are then undertaken to assess the opposite limiting case of nearly pure stochastic excitations. In the simulations, the harmonic amplitude is kept very small at $\underline{a} = 0.01 \text{ m/s}^2$ while the frequency is fixed at $\underline{\omega}_0$ / ω_0 =0.5. This frequency is selected since both dynamic regimes of snap-through and low amplitude intrawell dynamic behavior may occur for the nonlinear bistable energy harvester. Then, in addition to the small harmonic excitation contribution, the stochastic excitation component is set to have standard deviation in the range of $\sigma = [2, 4, 6, 8, 10]$ m/s². In order to obtain statistically reliable results for responses with stochastic characteristics, each data point presented in Fig. 4 corresponds to the mean value of 16 simulations that elapse for 600 excitation periods, and randomly chosen initial conditions to start each simulation run. The results are shown in Fig. 4. It is seen that under such nearly pure stochastic excitation scenario the overall rectified power generation from the energy harvester increases as the stochastic excitation standard deviation increases. Importantly, the rectified power demonstrates a dependence on the load resistor selection, achieving peak power levels for certain resistor values.

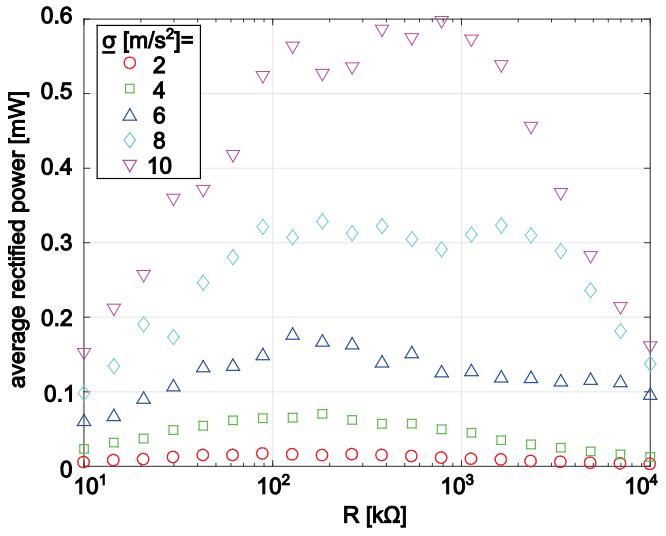


Figure 4. Simulation for the averaged rectified power generation from the nonlinear energy harvester under excitation with small harmonic contribution \underline{a} =0.01 m/s² and large stochastic component with varies standard deviation $\underline{\sigma}$ =[2, 4, 6, 8, 10] m/s², when harmonic frequency is at $\underline{\omega}_0$ / ω_0 =0.5, as functions of load resistor R.

Yet, the results of Fig. 4 do not suggest that a clear correlation exists between the resistor value and the DC power output since a distinct optimal resistance selection is not evident for gradually increasing noise standard deviation. Nevertheless,

the rectified power from the nonlinear harvester is maximized for resistances around $R = 10^2 \text{ k}\Omega$ to $R = 10^3 \text{ k}\Omega$ for almost each standard deviation of the stochastic excitation. These results encourage the continued investigation of how the trends of Fig. 4 are developed as an evolution from the opposite limiting case shown in Fig. 3 where the excitation is purely harmonic.

3.3 Rectified power generation under combinations of harmonic and stochastic excitation

Thus, the nonlinear energy harvester is subjected to a combination of harmonic and stochastic excitation with comparable amount of stochastic and harmonic components that span the two limiting cases. Figure 5 shows the results of rectified power generation when harmonic excitation has amplitude $a = 7.5 \text{ m/s}^2$ and frequency $\omega = 0.5$, while the standard deviation of stochastic excitation component varies such that the ratio between stochastic standard deviation and harmonic amplitude is $\sigma/a = [0, 0.5, 1, 1.5, 2]$. According to Fig. 5, without stochastic excitation, the power generation may have two different levels correspond to steady state snap-through and intrawell responses, similar to the results shown in Fig. 3. When the ratio of stochastic standard deviation and harmonic excitation amplitude is at $\sigma/a = 0.5$, the maximum rectified power is significantly decreased, from about 1.8 mW to 0.9 mW. In addition, the optimum resistor value that corresponds to maximum rectified power is also increased due to the introduction of stochastic excitation components. As the stochastic excitation level increases further, the maximum rectified power demonstrate a nearly linear increase. For instance, when the stochastic standard deviation to harmonic amplitude ratio is $\sigma / a = [0.5, 1, 1.5, 2]$ the maximum rectified power is respectively equal to [0.9, 1.15, 1.4, 1.75] mW. Moreover, the corresponding optimum resistor values also reduce for the same increase in the excitation ratio, revealing a particularly intricate trend needed to be uncovered for optimal deployment of such nonlinear energy harvesters in practical excitation scenarios.

An interesting observation is that when the stochastic standard deviation is twice the harmonic amplitude, the rectified power generation is almost the same as for the case that has only pure harmonic excitation, Fig. 5. To further investigate such factors, time series of AC voltage across the piezoelectric element and the DC voltage cross load resistor, corresponding to labeled points M and N in Fig. 5, are plotted in Fig. 6. According to Fig. 6(a), without the stochastic excitation contribution the nonlinear energy harvester is under steady state response with a nearly constant DC voltage across the load resistor. After the stochastic excitation component is introduced such that the ratio between noise standard deviation and harmonic amplitude is $\sigma / a = 2$ as shown in Fig. 6(b), the nonlinear energy harvester steady state response loses integrity, such that the rectified voltage varies considerably, although the mean rectified voltage level is similar to the case with pure harmonic excitation. The result suggests that a considerable amount of noise must be introduced to excite the nonlinear energy harvester in addition to the harmonic component so that the adverse effects of inhibiting snap-through dynamic behavior are overcome by large stochastic perturbations that trigger the behavior yet again.

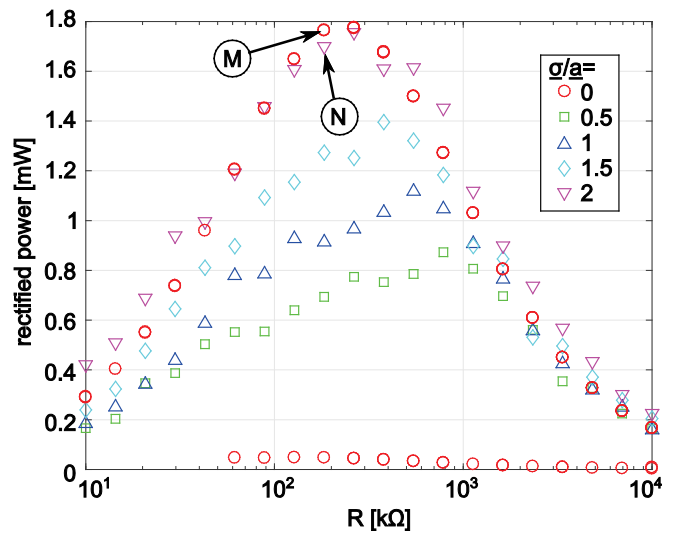


Figure 5. Numerical simulation for the rectified power generation from bistable energy harvester under combined excitation with harmonic amplitude \underline{a} =7.5 m/s² and frequency ω =0.5, and varies stochastic component such that the ratio between noise standard deviation and harmonic amplitude are $\underline{\sigma}/\underline{a}$ =[0, 0.5, 1, 1.5, 2], as functions of load resistor R.

4 CONCLUSION

To guide the effective implementation of nonlinear vibration energy harvesters in real world applications, this research uses a statistically significant set of numerical simulations to uncover the influences of load resistance and combined excitation characteristics on the DC power delivery from nonlinear vibration energy harvesters. The limiting cases of pure harmonic or nearly pure stochastic excitations help to identify the overall trends in power generation from such pure, yet not common, excitation scenarios. Yet, when the harvester is driven by excitations that combine harmonic and stochastic components. the maximum rectified power and optimum resistor reveal mutual dependence on the ratio of stochastic to harmonic excitation levels. By providing important first light on the intricate problem at hand, these simulation results motivate continued studies by alternative and more rigorous methods, such as analysis [13], that conclusively identify optimal operating conditions and designs of the nonlinear energy harvesting system for DC power delivery in real world contexts.

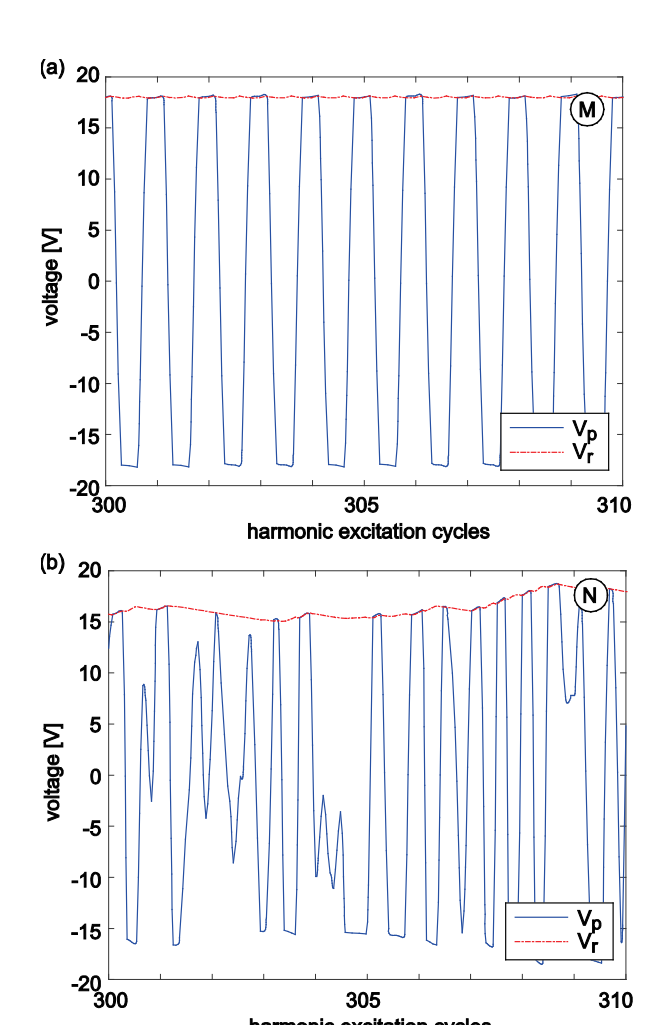


Figure 6. Time series of piezoelectric element voltage and rectified voltage across resistive load R =183.3 k Ω when the ratio of stochastic standard deviation and harmonic amplitude is (a) $\underline{\sigma}/\underline{a}$ =0 and (b) $\underline{\sigma}/\underline{a}$ =2, corresponding to points as indicated by label M and N from Fig. 5.

harmonic excitation cycles

ACKNOWLEDGEMENTS

This research is supported by The Ohio State University Center for Automotive Research..

REFERENCES

- [1] R.B. Randall, *Vibration-based Condition Monitoring: Industrial, Aerospace and Automotive Applications* (Wiley, Chichester, 2011).
- [2] K. Baert, et al., Technologies for highly miniaturized autonomous sensor networks, *Microelectronics Journal* **37**, 1563-1568 (2006).
- [3] P.L. Green, E. Papatheou, N.D. Sims, Energy harvesting from human motion and bridge vibrations: an evaluation of current nonlinear energy

- harvesting solutions, *Journal of Intelligent Material Systems and Structures* **24**, 1494-1505 (2013).
- [4] J.D. Turner, A.J. Pretlove, A study of the spectrum of traffic-induced bridge vibration, *Journal of Sound and Vibration* **122**, 31-42 (1988).
- [5] S. Leadenham, A. Erturk, M-shaped asymmetric nonlinear oscillator for broadband vibration energy harvesting: harmonic balance analysis and experimental validation, *Journal of Sound and Vibration* **333**, 6209-6223 (2014).
- [6] B.P. Mann, N.D. Sims, Energy harvesting from the nonlinear oscillations of magnetic levitation, *Journal of Sound and Vibration* **319**, 515-530 (2009).
- [7] F. Cottone, H. Vocca, L. Gammaitoni, Nonlinear energy harvesting, *Physical Review Letters* **102**, 080601 (2009).
- [8] L. Tang, Y. Yang, C.K. Soh, Toward broadband vibration-based energy harvesting, *Journal of Intelligent Material Systems and Structures* 21, 1867-1897 (2010).
- [9] S.C. Stanton, C.C. McGehee, B.P. Mann, Nonlinear dynamics for broadband energy harvesting: investigation of a bistable piezoelectric inertial generator, *Physica D* **239**, 640-653 (2010).
- [10] A. Erturk, D.J. Inman, Broadband piezoelectric power generation on high-energy orbits of the bistable Duffing oscillator with electromechanical coupling, *Journal of Sound and Vibration* 330, 2339-2353 (2011).
- [11] R. Masana, M.F. Daqaq, Relative performance of a vibratory energy harvester in mono- and bi-stable potentials, *Journal of Sound and Vibration* **330**, 6036-6052 (2011).
- [12] M. Panyam, R. Masana, M.F. Daqaq, On approximating the effective bandwidth of bi-stable energy harvesters, *International Journal of Non-Linear Mechanics* **67**, 153-163 (2014).
- [13] R.L. Harne, K.W. Wang, *Harnessing Bistable Structural Dynamics: for Vibration Control, Energy Harvesting and Sensing* (John Wiley & Sons Ltd., Chichester, 2017).
- [14] S. Roundy, P.K. Wright, J. Rabaey, A study of low level vibrations as a power source for wireless sensor nodes, *Computer Communications* **26**, 1131-1144 (2003).
- [15] A. Erturk, D.J. Inman, *Piezoelectric Energy Harvesting* (Wiley, Chichester, 2011).

- [16] C.B. Williams, R.B. Yates, Analysis of a microelectric generator for microsystems, *Sensors and Actuators A* **52**, 8-11 (1996).
- [17] P. Glynne-Jones, M.J. Tudor, S.P. Beeby, N.M. White, An electromagnetic, vibration-powered generator for intelligent sensor systems, *Sensors and Actuators A* **110**, 344-349 (2004).
- [18] A. Erturk, D.J. Inman, An experimentally validated bimorph cantilever model for piezoelectric energy harvesting from base excitations, *Smart Materials and Structures* **18**, 025009 (2009).
- [19] S.C. Stanton, B.A.M. Owens, B.P. Mann, Harmonic balance analysis of the bistable piezoelectric inertial generator, *Journal of Sound and Vibration* **331**, 3617-3627 (2012).
- [20] M. Panyam, M.F. Daqaq, A comparative performance analysis of electrically optimized nonlinear energy harvesters, *Journal of Intelligent Material Systems and Structures* **27**, 537-548 (2016).
- [21] M.F. Daqaq, Transduction of a bistable inductive generator driven by white and exponentially correlated Gaussian noise, *Journal of Sound and Vibration* **330**, 2554-2564 (2011).
- [22] R.L. Harne, K.W. Wang, Prospects for nonlinear energy harvesting systems designed near the elastic stability limit when driven by colored noise, *ASME Journal of Vibration and Acoustics* **136**, 021009 (2014).
- [23] Y.G. Leng, Y.J. Gao, D. Tan, S.B. Fan, Z.H. Lai, An elastic-support model for enhanced bistable piezoelectric energy harvesting from random vibrations, *Journal of Applied Physics* **117**, 064901 (2015).
- [24] N. Kong, D.S. Ha, A. Erturk, D.J. Inman, Resistive impedance matching circuit for piezoelectric energy harvesting, *Journal of Intelligent Material Systems and Structures* **21**, 1293-1302 (2010).
- [25] Y.C. Shu, I.C. Lien, Efficiency of energy conversion for a piezoelectric power harvesting system, *Journal of Micromechanics and Microengineering* **16**, 2429-2438 (2006).
- [26] Y.C. Shu, I.C. Lien, W.J. Wu, An improved analysis of the SSHI interface in piezoelectric energy harvesting, *Smart Materials and Structures* **16**, 2253-2264 (2007).
- [27] J. Liang, W.H. Liao, Impedance modeling and analysis for piezoelectric energy harvesting systems,

- *IEEE/ASME Transactions on Mechatronics* **17**, 1145-1157 (2012).
- [28] Y. Wu, A. Badel, F. Formosa, W. Liu, A.E. Agbossou, Piezoelectric vibration energy harvesting by optimized synchronous electric charge extraction, *Journal of Intelligent Material Systems and Structures* **24**, 1445-1458 (2012).
- [29] E. Lefeuvre, A. Badel, C. Richard, Piezoelectric energy harvesting device optimization by synchronous electric charge extraction, *Journal of Intelligent Material Systems and Structures* **16**, 865-876 (2005).
- [30] Y.C. Shu, I.C. Lien, Analysis of power output for piezoelectric energy harvesting systems, *Smart Materials and Structures* **15**, 1499-1512 (2006).
- [31] SG-Link-LXRS Wireless 2 Channel Analog Input Sensor Node. User Manual. Willston, Vermont: LORD Corporation; 2015.
- [32] H.A. Sodano, D.J. Inman, G. Park, Comparison of piezoelectric energy harvesting devices for recharging batteries, *Journal of Intelligent Material Systems and Structures* **16**, 799-807 (2005).
- [33] L. Zuo, P.S. Zhang, Energy harvesting, ride comfort, and road handling of regenerative vehicle suspensions, *Journal of Vibration and Acoustics* **135**, 011002 (2013).
- [34] F.C. Moon, P.J. Holmes, A magnetoelastic strange attractor, *Journal of Sound and Vibration* **65**, 275-296 (1979).
- [35] M. Schaeffer, M. Ruzzene, Wave propagation in multistable magneto-elastic lattices, *International Journal of Solids and Structures* **56-57**, 78-95 (2015).
- [36] T. Hikihara, T. Kawagoshi, An experimental study on stabilization of unstable periodic motion in magneto-elastic chaos, *Physics Letters A* **211**, 29-36 (1996).
- [37] B.F. Feeny, C.M. Yuan, Parametric identification of an experimental magneto-elastic oscillator, *Journal* of Sound and Vibration 247, 785-806 (2001).
- [38] R.L. Harne, K.W. Wang, On the fundamental and superharmonic effects in bistable energy harvesting, *Journal of Intelligent Material Systems and Structures* **25**, 937-950 (2014).
- [39] L.N. Virgin, *Vibration of Axially Loaded Structures* (Cambridge University Press, Cambridge, 2007).

[40] J.B. Roberts, P.D. Spanos, *Random Vibration and Statistical Linearization* (Wiley, New York, 1990).